

# Functional morphology and biomechanics of the tongue-bite apparatus in salmonid and osteoglossomorph fishes

Ariel L. Camp,<sup>1</sup> Nicolai Konow<sup>1,2</sup> and Christopher P. J. Sanford<sup>1</sup>

<sup>1</sup>Department of Biology, Hofstra University, Hempstead, NY, USA

<sup>2</sup>Currently at Johns Hopkins University, Department of Physical Medicine and Rehabilitation, 98 N. Broadway, Suite 409, Baltimore, MD 21231, USA

## Abstract

The tongue-bite apparatus and its associated musculoskeletal elements of the pectoral girdle and neurocranium form the structural basis of raking, a unique prey-processing behaviour in salmonid and osteoglossomorph fishes. Using a quantitative approach, the functional osteology and myology of this system were compared between representatives of each lineage, i.e. the salmonid *Salvelinus fontinalis* ( $N = 10$ ) and the osteoglossomorph *Chitala ornata* ( $N = 8$ ). Divergence was found in the morphology of the novel cleithrobranchial ligament, which potentially relates to kinematic differences between the raking lineage representatives. *Salvelinus* had greater anatomical cross-sectional areas of the epaxial, hypaxial and protractor hyoideus muscles, whereas *Chitala* had greater sternohyoideus and adductor mandibulae mass. Two osteology-based biomechanical models (a third-order lever for neurocranial elevation and a modified four-bar linkage for hyoid retraction) showed divergent force/velocity priorities in the study taxa. *Salvelinus* maximizes both force (via powerful cranial muscles) and velocity (through mechanical amplification) during raking. In contrast, *Chitala* has relatively low muscle force but more efficient force transmission through both mechanisms compared with *Salvelinus*. It remains unclear if and how behavioural modulation and specializations in the post-cranial anatomy may affect the force/velocity trade-offs in *Chitala*. Further studies of tongue-bite apparatus morphology and biomechanics in a broader species range may help to clarify the role that osteology and myology play in the evolution of behavioural diversity.

**Key words** behaviour; biomechanics; feeding; fish; four-bar linkage; levers; modulation.

## Introduction

Bony fish feeding behaviours have in the past provided useful model systems of the influence of morphology on biomechanics, phylogeny and behaviours (Muller, 1987; Wainwright, 1988; Westneat, 1994, 2003). Although several studies focused on prey capture, a structurally and functionally novel prey-processing behaviour (raking) has been identified via functional studies of kinematics and motor activity patterns in two evolutionarily distinct lineages, i.e. the more derived salmonids and the basal teleostean osteoglossomorphs (Sanford & Lauder, 1989, 1990; Sanford, 2001a,b; Konow & Sanford, 2008a,b; Konow et al. 2008).

Raking is accomplished via entirely novel prey-processing movements in the tongue-bite apparatus (TBA), which is formed by teeth on the oral or dorsal side of the basihyal (tongue) (the TBA lower jaw) and the ventral side of the

neurocranium or roof of the oral cavity (the TBA upper jaw) (Lauder & Liem, 1983; Sanford & Lauder, 1989, 1990; Hilton, 2001, 2003). Following capture, the prey is stabilized by occlusion of the mandibular jaws, and neurocranial elevation then rotates the TBA upper jaw anterodorsally. Concomitant pectoral girdle retraction moves the TBA lower jaw posterodorsally, resulting in inversely directed shearing of the TBA jaws, thus raking the prey (Konow et al. 2008).

Although anatomical descriptions of cranial and jaw osteology and myology in representative species of each lineage are abundant (Ridewood, 1904; Taverne, 1978; Sanford, 2000; Lauder & Liem, 1983; Hilton, 2001; Konow & Sanford, 2008a,b), no quantitative or comparative morphological study of the TBA between the lineages exists. Knowledge of the key morphological differences between these lineages will provide important information to determine how structural changes can directly influence novel functions (Lauder, 1985; Galis, 2001). Therefore, the osteology and myology of the TBA and associated structures are compared herein, between the salmonid brook trout *Salvelinus fontinalis* (Mitchill, 1814) and the osteoglossomorph clown knifefish *Chitala ornata* (Gray, 1831). The

### Correspondence

Ariel L. Camp, Department of Biology, 114 Hofstra University, Hempstead, NY 11549, USA. E: ariel.l.camp@gmail.com

Accepted for publication 16 January 2009

overall aim was to quantify any functionally important differences between these taxa. Both are relatively basal species within their lineages, yet sufficiently derived to ensure that all relevant morphological specializations are present. Although both use suction-feeding prey-capture strategies, the study taxa vary significantly in their raking kinematics and behaviour. *Chitala* relies primarily on pectoral girdle retraction augmented by neurocranial elevation (Sanford & Lauder, 1989, 1990; Frost & Sanford, 1999), and modulates both its raking kinematics and muscle activity pattern when engaging different prey types (Konow et al. 2008). In contrast, *Salvelinus* utilizes extensive neurocranial elevation, as well as pectoral girdle retraction comparable to that of *Chitala*, in a raking behaviour that is remarkably stereotypical in both its kinematics and muscle activity patterns (Sanford, 2001b; Konow et al. 2008).

Two complementary biomechanical models are proposed to govern raking kinematics (Konow & Sanford, 2008b), primarily based on kinematic observations (Frost & Sanford, 1999; Sanford & Lauder, 1989, 1990; Sanford, 2001a,b). Neurocranial elevation during the raking power-stroke has been modelled previously by a simple, third-order lever (e.g. Carroll, 2004; Grubich, 2005). Meanwhile, hyoid retraction can be described via the planar four-bar linkage proposed for hyoid depression by Muller (1987) (see also Konow & Sanford, 2008b). The trade-off between force and velocity in both of these complementary biomechanical mechanisms is directly influenced by structural differences and focusing on such trade-offs can provide important insights into musculo-skeletal design (Westneat, 2003, 2004).

We aimed to quantify the linkage osteology and myology to provide a detailed evaluation of the utility of these biomechanical models in predicting raking functional morphology. As *Salvelinus* is a trophic generalist but does not show kinematic modulation, it is hypothesized that the TBA of *Salvelinus*, in contrast to *Chitala*, has structural and mechanical characteristics that optimize the raking power-stroke without modulation (Sanford, 2001a). The present study will therefore be key in evaluating (1) whether interspecific differences in mechanical, osteological and myological components of an organism explain reported divergence in behaviours and (2) what predictions the proposed third-order lever and planar four-bar linkage pose about TBA function and the interplay between force/velocity trade-offs and structural design.

## Materials and methods

### Study taxa

Size-matched specimens of *Salvelinus* ( $N = 10$ ) and *Chitala* ( $N = 8$ ) were obtained live from Cold Spring Harbor Fish Hatchery (NY, USA) and Long Island Aquatics (NY, USA) and killed in an alcoholic solution of clove oil (Eugenol). For each individual, total length, standard length, head length and total body mass were recorded

(Table 1). Head lengths (*Salvelinus*, 40.0 mm, S.E.M.  $\pm$  1.16 mm,  $N = 10$ ; *Chitala*, 38.8 mm, S.E.M.  $\pm$  2.16 mm,  $N = 8$ ) were not statistically different in these specimens ( $t$ -test;  $P = 0.1$ ). This close size-matching of specimens, which were within the juvenile stage for both species, was intentional in order to avoid scaling issues (e.g. Wainwright & Richard, 1995) and effects of ontogeny in our dataset.

### Osteological measurement protocol

All osteological terminology follows Gregory (1933). Osteological measurements were taken using dial calipers on the freshly killed specimens in order to most accurately represent natural tissue morphology and feeding apparatus movement and flexibility. Cranial length, from the rostrum to the posterior-most edge of the neurocranium, was measured but used only as a size metric, similar to head length, which extended from the rostrum to the furthest posterior margin of the pectoral girdle. The protocol for measurements of osteological variables (Fig. 1B) was designed to exhaustively quantify the integral TBA bony elements described in earlier functional studies (Sanford & Lauder, 1989, 1990; Sanford, 2000; Hilton, 2001, 2003) and the proposed link components of the biomechanical models (Konow & Sanford, 2008b).

The TBA length [(1) in Fig. 1B] was the distance from the anterior-most point of the basihyal to the furthest posterior margin of the pectoral girdle. Basihyal depth (2) was measured at the maximum dorsoventral depth of the basihyal. Inverse epaxial distance (7) was measured as the distance from the craniovertebral joint to the ventral margin of the cranium. The pectoral girdle was described by measuring the length of the cleithrum (9).

The third-order lever for neurocranial elevation consists of the in-lever, defined as the distance between the craniovertebral joint and the centroid of the epaxial muscle insertion (Carroll et al. 2004). This value was calculated using half the distance from the craniovertebral joint to the dorsal-most possible epaxial insertion point on the neurocranial crest (6). The out-lever (8) extends from the craniovertebral joint to the anterior-most tooth of the parasphenoid or vomerine dentition forming the dorsal TBA jaw.

The proposed four-bar linkage was quantified through link length measurements consisting of the fixed link (10) (formed by the hyomandibular and neurocranium, extending from the interhyal to the craniovertebral joint), the input link (5) (measured from the ventral edge of the anteroventral-most projection of the post-temporal to the anteroventral-most pectoral girdle edge), the coupler link (4) [comprising the sternohyoideus (SH) muscle with the cleithrobranchial ligament (CBL), from the anteroventral tip of the cleithrum to the basihyal articulation with the anterior ceratohyal] and the output link (3) (from the articulation of the basihyal with the ceratohyal to the interhyal articulation with the hyomandibular). The dorsal tip of the input link does not meet the dorsal tip of the fixed link as measured in this protocol, a situation that is not unprecedented in biological applications of four-bar linkages (Muller, 1987). However, the offset between the dorsal tips of these two links (i.e. the distance from the anteroventral-most projection of the post-temporal and the craniovertebral joint) was considered minimal and not biologically significant.

### Myology measurement protocol

We measured the unilateral and unpreserved muscle mass and anatomical cross-sectional area (ACSA) in five cranial muscles of known importance in powering raking behaviours (Sanford & Lauder, 1989; Konow & Sanford, 2008a), i.e. the  $A_2A_3$  section of

**Table 1** Means and S.E. measurements ( $N = 10$  for *Salvelinus* and  $N = 8$  for *Chitala*) for osteological and myological measurements of the tongue-bite apparatus (TBA) and related structures in *Salvelinus* and *Chitala*

	Measurement	<i>Salvelinus</i>		<i>Chitala</i>	
		Mean	S.E.M.	Mean	S.E.M.
Morphometrics	Total length (mm)	184.60	4.70	174.80	10.80
	Standard length (mm)	155.68	4.39	160.25	10.11
	Head length (mm)	39.97	1.16	38.78	2.16
	Cranial length (mm)	27.84	0.83	30.43	1.36
	Total body mass (g)	60.06	3.84	37.88	5.75
Osteology	(1) TBA length (mm)	36.07	1.08	34.56	1.74
	(2) Basihyal depth (mm)	4.36	0.21	3.34	0.19
	(3) Four-bar output link (mm)	17.37	0.64	16.15	0.91
	(4) Four-bar coupler link (mm)	27.58	1.46	25.56	2.34
	(5) Four-bar input link (mm)	19.87	1.55	26.86	2.10
	(6) Cranial in-lever (mm)	10.24	0.57	10.91	0.59
	(7) Inverse epaxial distance (mm)	4.21	0.23	3.78	0.34
	(8) Cranial out-lever (mm)	24.70	0.68	17.51	1.01
	(9) Cleithrum length (mm)	12.18	0.87	18.42	1.12
	(10) Four-bar fixed link (mm)	16.24	0.57	16.78	1.49
Myology	Supracleithrum length (mm)*	10.27	0.58	6.83	0.59
	Post-temporal length (mm)*	9.60	0.62	7.79	0.44
	AM ACSA (mm <sup>2</sup> )	37.63	3.84	30.41	4.23
	AM mass (g)	0.28	0.02	0.22	0.04
	PH ACSA (mm <sup>2</sup> )	9.84	0.46	6.52	0.97
	PH mass (g)	0.12	0.01	0.07	0.01
	SH ACSA (mm <sup>2</sup> )	24.43	3.36	20.40	2.23
	SH mass (g)	0.15	0.02	0.18	0.03
	EP ACSA (mm <sup>2</sup> )	99.77	6.70	74.20	6.86
	EP mass (g)	0.54	0.07	0.41	0.08
	HP ACSA (mm <sup>2</sup> )	118.96	8.27	57.07	3.40
	HP mass (g)	0.44	0.03	0.34	0.06

\*Measured but not included in parametric analyses (see text). ACSA, anatomical cross-sectional area; AM, adductor mandibularis; EP, epaxialis; HP, hypaxialis; PH, protractor hyoideus; SH, sternohyoideus. Bracketed numbers for osteological measurements correspond to the location of the measurement in Fig. 1B.

the adductor mandibularis (AM), constituting the entire AM in these basal teleosts (Lauder & Liem, 1980), epaxialis (EP) muscles, hypaxialis (HP) muscles, sternohyoideus (SH), protractor hyoideus (PH) in *Salvelinus* and its functional equivalent, the posterior intermandibularis (PIM), in *Chitala* (Greenwood, 1971) (Fig. 2A,C).

Muscles of interest were excised, placed in isotonic saline for rehydration and sequentially blotted dry before weighing on a Mettler scale (Acculab model 167555, calibrated to 0.01 g). Anatomical cross-sections were cut perpendicular to the prevalent fibre orientation in each muscle, the determination of which was visually aided by dripping Lugol's solution onto the muscle under an Olympus SZX12 dissecting microscope and camera. For sections of the AM, PH/PIM and SH, the cross-sectional cut was made through the belly of the muscle midway between the origin and insertion (Fig. 2A,C). Although evidence exists that the posterior regions of the HP and EP muscles may be recruited during feeding (Thys, 1997), previous electromyographical studies of *Salvelinus* and *Chitala* have only sampled the anterior section of these muscles (Lauder & Liem, 1983; Sanford & Lauder, 1989; Konow et al. 2008). Therefore, we focused on the anterior-most portions of the EP and HP to ensure functional comparability between this study and

existing raking muscle activity evidence. A dorsoventral incision was made 3.0 mm caudal to the posterior-most margin of the pectoral girdle, and only the HP and EP muscle anterior to this plane was used for mass measurements and to obtain ACSAs (Fig. 2A,C).

All cross-sections were taken from left side muscles, placed with the cut plane, which was perpendicular to muscle fibre orientation, facing up and photographed with a scale bar using a digital camera (Canon PowerShot A80) mounted with the lens axis perpendicular to the muscle section. Finally, scaled ACSA measurements were obtained from these photographs using the lasso tool in ImageJ 1.37.

Tissue-cleared and counter-stained preparations for bone and cartilage were prepared from a size range of formalin-fixed specimens of each taxon, distinct from the size-matched specimens used above for morphological measurements, using a combined trypsin and KOH protocol (see Konow & Bellwood, 2005). These specimens were dissected step-wise and photographed using the Olympus dissecting microscope. Anatomical diagrams (Fig. 3) were prepared from the resulting photographs by tracing bony, muscular and connective tissue elements in Corel Draw v. 12.0 (Corel Corp., 2006). Inspections of these specimens also formed the major basis for assessing ontogenetic trait variability, including

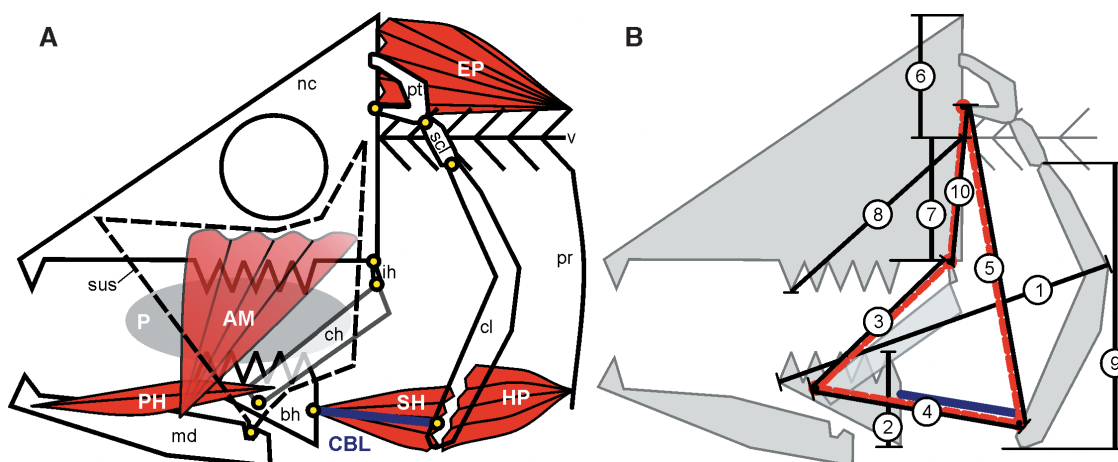


**Fig. 1** (A) Diagram of generalized osteology and myology of the tongue-bite apparatus (TBA) and associated structures in a teleost fish. In *Chitala* the posterior intermandibularis is the functional equivalent of the protractor hyoideus (PH) in *Salvelinus* (Greenwood, 1971). Other myology: AM, adductor mandibularis; CBL, cleithrobranchial ligament; EP, epaxialis; HP, hypaxialis; SH, sternohyoideus. Osteology: bh, basihyal; ch, ceratohyal; cl, cleithrum; ih, interhyal; md, mandible; nc, neurocranium; pr, pleural rib; pt, post-temporal; scl, supraclithrum; sus, suspensorium; v, vertebral column. P indicates prey. (B) Osteological measurements obtained from dissected individuals (see text for anatomical descriptions). 1, TBA length; 2, maximum basihyal depth; 3, four-bar output link; 4, four-bar coupler link; 5, four-bar input link; 6, cranial in-lever; 7, inverse epaxialis distance; 8, cranial out-lever; 9, cleithrum length; 10, four-bar fixed link.

TBA dentition measurements. Such assessments, along with non-parametric statistical tests, guided subsequent decisions of whether it was functionally appropriate to exclude traits from the parametric analyses of our morphometric datasets (see below).

### Biomechanical calculations

To facilitate direct comparison, in both the third-order lever and four-bar linkage models it is assumed that all forces are perpendicular to their respective lever and link elements. For the third-order lever, the mechanical advantage (MA) and its inverse the displacement advantage (DA) represent the proportion of force and velocity, respectively, transmitted from the EP muscle to the neurocranium (Grubich, 2005). MA was calculated as the ratio of cranial in-lever (half of measurement 6, Fig. 1B) to out-lever (measurement 8, Fig. 1B) length from each individual (Table 1), scaled to cranial length. Given that muscle force is proportional to cross-sectional area (Grubich, 2005), the input force of the neurocranial lever can be approximated by the EP ACSA. Thus, the theoretical output force of this lever in each species was estimated by multiplying the species-mean EP ACSA by the MA of the third-order lever.

Similarly, values of force and velocity transmission were calculated for the four-bar linkage; the force transmission coefficient (FT) and its inverse the kinematic transmission coefficient (KT) represent amplification of input torque and velocity, respectively (Tao, 1967; Westneat, 1994) delivered to the basihyal (Suh & Radcliffe, 1978). To examine the output force transmitted through the four-bar linkage, an output force factor (OFF) was calculated for each species by multiplying the ratio of input link to output link lengths by the FT value (Aerts & Verraes, 1984). Following Anker (1974), FT was calculated as the ratio of input rotation to output rotation, with KT being the inverse ratio. Input rotation was defined as the angular change between the input and fixed links from the onset of the rake (Fig. 3B,E) to the maximum displacement of the

neurocranium and pectoral girdle (Fig. 3C,F), and output rotation as the change in the angle between the fixed and output links over the same time period. Kinematic data from both species (Sanford & Lauder, 1990; Sanford, 2001b; Konow et al. 2008) were used to obtain the input angles (Fig. 4). Output angles were calculated from the input angles using the laws of sines and cosines and the four-bar link lengths measured herein (Fig. 4). Because solving these trigonometric equations gives two possible output angles, for each species the two possible calculated output angles were compared with the kinematic data (Sanford & Lauder, 1990; Sanford, 2001b; Konow et al. 2008) and the output angle that most closely matched observed hyoid motion was chosen. For *Salvelinus*, the tendency of the coupler link to change length when stretched led to possible overestimation of its length if elements of the TBA were stretched during measurement. In four individuals of *Salvelinus*, the measured coupler link length had to be shortened by  $\leq 5.5$  mm in order to render the four-bar linkage physically possible given the initial input angle measured from kinematic data (see above). The ability of a four-bar link to change length is not unprecedented (Muller, 1987) and length changes greater than 5.5 mm are seen in coupler link length during raking behaviour in *Salvelinus* (Konow and Camp, unpublished data).

### Statistical analyses

Mean and S.E. measurements were calculated for all measured variables (Table 1) and  $r^2$  values were obtained from linear regressions against head length for osteology variables and against body mass for myology variables. Variables with low  $r^2$  values indicated high intraspecific variation, and when our evaluations of their functional significance deemed such exclusion appropriate these variables were removed from further analysis.

Pearson correlations were also performed on the variable matrix; supraclithrum length and post-temporal length returned Pearson

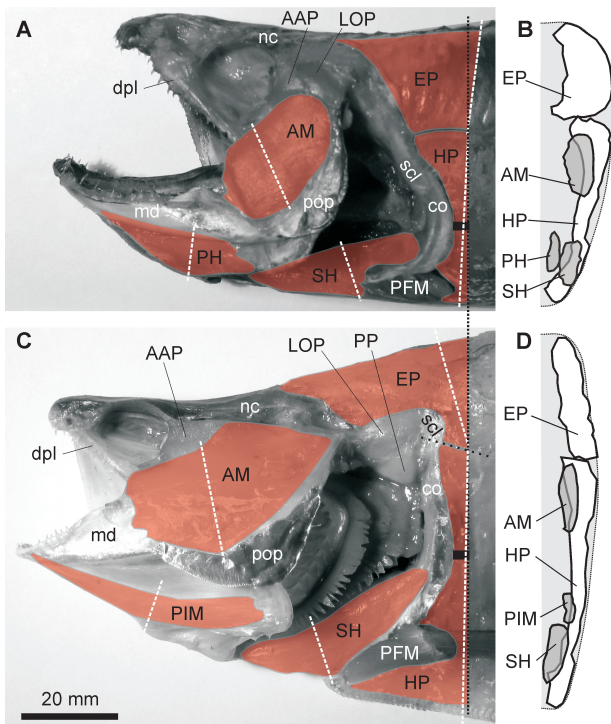


**Fig. 2** Scaled diagram showing lateral views of cranial muscles associated with raking behaviour in *Salvelinus* (A) and *Chitala* (C) after removal of suspensorium, maxilla, lower jaw and operculum and an anterior view of anatomical cross-sectional area (ACSA) of cranial muscles in *Salvelinus* (B) and *Chitala* (D). Dashed white lines indicate the plane and orientation of ACSA; dotted black lines indicate posterior expanse of epaxialis (EP) and hypaxialis (HP) musculature quantified, with the black bar indicating the 3.0 mm caudal displacement from the pectoral girdle of the EP and HP excision. Myology: AAP, adductor arcus palatine; AM, adductor mandibularis; LOP, levator opercularis; PFM, pectoral fin muscle; PIM, posterior intermandibularis; PH, protractor hyoideus; PP, protractor pectoralis; SH, sternohyoideus. Osteology: co, cleithrum; dpl, dermopalatine; md, mandible; nc, neurocranium; pop, pre-opercular; scl, supracleithrum.

correlations  $> 0.7$  with cleithrum length (i.e. the pectoral girdle proper). Guided by previous functional studies, we assumed that cleithrum length is over-ridingly functionally significant, and the two former variables were therefore also excluded from further analysis, whereas cleithrum length was retained. All remaining linear measurements (Table 2) were divided by cranial length and  $\log_{10}$ -transformed prior to further statistical analyses. Muscle masses were divided by total body mass and the ratio was  $\log_{10}$ -transformed. ACSAs were divided by total body mass and square-root transformed.

We ran a principal component analysis (PCA) constrained to four axes, each with Eigenvalues  $\geq 1$  on the correlation matrix of the transformed dataset (Systat v. 11.0). This analysis identified the variables responsible for driving overall differences in TBA morphology. MANOVAs on the resulting principal component (PC) factor scores (Table 2) tested for a significant effect of species, followed by univariate ANOVAs to establish which axes of the PCA contributed significantly to interspecific variation. Variables with PC loadings  $> 0.5$  along the significant axis were considered important in separating the two taxa.

**Table 2** Principal component (PC) loadings of osteological and myological variables for *Chitala* and *Salvelinus* resulting from a PC analysis, with significant loadings ( $> 0.5$ ) along PC1 in bold

Measurement variable	PC1	PC2	PC3	PC4
(8) Cranial out-lever	<b>0.927</b>	0.043	-0.247	-0.103
HP ACSA	<b>0.902</b>	-0.225	-0.073	-0.079
(2) Basihyal depth	<b>0.822</b>	0.096	-0.069	0.273
(3) Four-bar output link	<b>0.769</b>	0.140	0.009	0.106
(9) Cleithrum length	<b>-0.761</b>	-0.350	0.263	0.096
(1) TBA length	<b>0.751</b>	0.070	0.082	0.278
SH mass	<b>-0.745</b>	0.089	0.389	0.237
PH ACSA	<b>0.730</b>	-0.397	0.225	0.261
EP ACSA	<b>0.616</b>	-0.456	0.290	-0.306
(4) Four-bar coupler link	<b>0.577</b>	0.215	0.299	0.091
(10) Four-bar fixed link	<b>0.566</b>	-0.282	0.544	-0.287
(7) Inverse epaxial distance	<b>0.553</b>	0.551	0.310	0.038
(5) Four-bar input link	<b>-0.525</b>	-0.684	0.129	0.142
AM mass	<b>-0.509</b>	-0.177	0.584	0.293
SH ACSA	0.310	-0.648	0.337	0.053
HP mass	-0.191	0.605	0.296	0.122
EP mass	-0.183	0.595	0.318	-0.233
(6) Cranial in-lever	0.161	0.580	0.401	0.007
AM ACSA	0.432	-0.499	0.534	-0.003
PH mass	-0.054	0.028	0.120	0.804
Percent of total variance	35.2	15.6	12.7	6.9
Univariate ANOVAs <i>P</i> -values	<b>&lt; 0.001</b>	<b>&gt; 0.05</b>	<b>&gt; 0.05</b>	<b>&gt; 0.05</b>

ACSA, anatomical cross-sectional area; AM, adductor mandibularis; EP, epaxialis; HP, hypaxialis; PH, protractor hyoideus; SH, sternohyoideus; TBA, tongue-bite apparatus. The variables are listed in order of magnitude of the PC loadings along axis 1. Positive component loadings along PC1 signify variables with greater values in *Salvelinus* and negative component loadings signify those with greater values in *Chitala*. *P*-values are from univariate ANOVAs on the PC scores along each PC axis, with bold indicating statistical significance. Bracketed numbers for osteological measurements correspond to the location of the measurement in Fig. 1B.

## Results

### Qualitative tongue-bite apparatus morphology

The cranial osteology and myology of *Salvelinus* have been thoroughly described (Rosen, 1974, 1985; Sanford, 2000; Lauder & Liem, 1980) and vary little from that of the rainbow trout, *Oncorhynchus mykiss*, for which the structural and functional aspects of the TBA were recently described by Konow & Sanford (2008b). In *Chitala*, the cranial osteology (Ridewood, 1904; Greenwood, 1971, 1973; Taverne, 1978; Sanford & Lauder, 1989) and the morphology of the TBA (Hilton, 2001) have also been examined. Therefore, we only treat morphological aspects that are considered relevant to the present study in the following description.

Both species possess prominent fang-like basihyal dentition with a predominately posterodorsal tooth

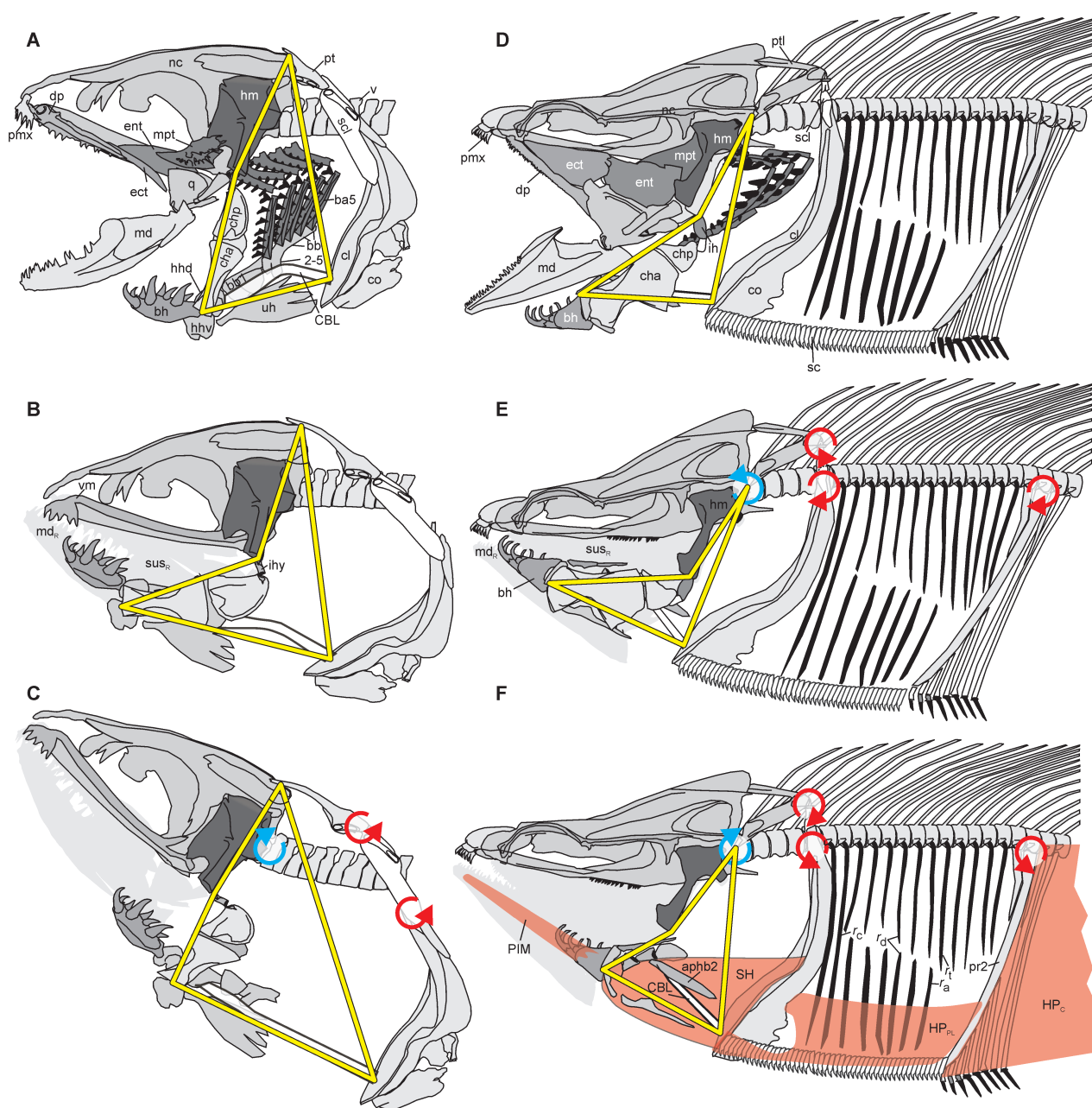


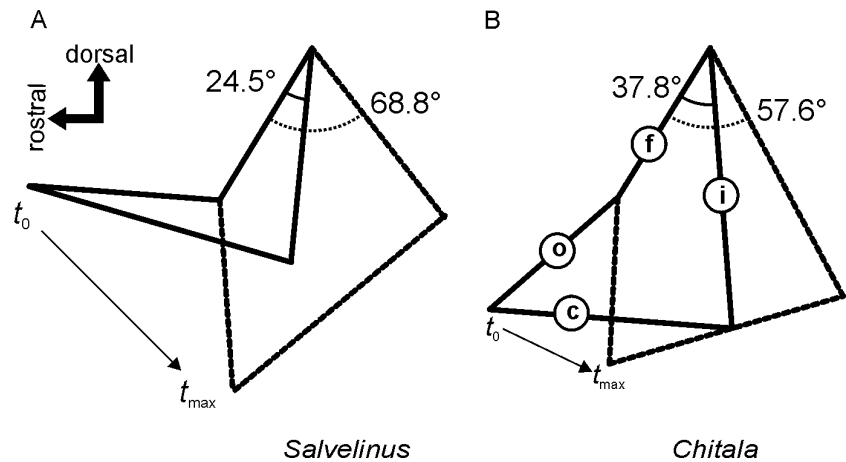
**Fig. 3** Position of osteological elements of the tongue-bite apparatus and relevant post-cranial structures at the strike (A and D), onset of rake (B and E) and maximum pectoral girdle and neurocranial excursion during rake (C and F) in *Salvelinus* (A–C) and *Chitala* (D–F). Approximate configuration of planar four-bar linkage at each position is show in yellow; blue arrows indicate direction and point of rotation for movements resulting in neurocranial kinesis, whereas red arrows show direction and point of rotation for movements resulting in pectoral girdle kinesis. Subscript ‘R’ indicates right (far) side of individual. abph2, autogenous bony process of second basibranchial; ba5, fifth basibranchial; bb1, first basibranchial; bb2, second basibranchial; bh, basihyal; CBL, cleithrobranchial ligament; cha, anterior ceratohyal; chp, posterior ceratohyal; cl, cleithrum; co, coracoid; dp, dermopalatine; ect, ectopterygoid; ent, entopterygoid; hm, hyomandible; hhv, ventral hypohyal; hhd, dorsal hypohyal; HP<sub>c</sub>, caudal hypaxialis; HP<sub>r</sub>, pleural hypaxialis; ihy, interhyal; md, mandible; mpt, metapterygoid; nc, neurocranium; pmx, pre-maxilla; pr2, second anal pterygiophore; pt, post-temporal; q, quadrate; r, pleural rib (r<sub>a</sub>, autogenous pleural rib; r<sub>c</sub>, continuous pleural rib; r<sub>d</sub>, discontinuous pleural rib; r<sub>t</sub>, true pleural rib); sc, scutes; scl, supracleithrum; sus, suspensorium; v, vertebral column; vm, vomer.

curvature (Fig. 3). In *Salvelinus*, the TBA upper jaw dentition is restricted to the anterior vomerine surface and consists of anteroventrally recurved, fang-like teeth arranged in an anteriorly pointing triangle (Fig. 3B). In contrast, *Chitala*

has straight, caniniform teeth arranged along the posterior parasphenoid midline (Fig. 3E).

Both taxa possess CBLs originating on the cleithrum close to the midline. The ligament is elongate and follows

**Fig. 4** Change in four-bar confirmation and the angle between the fixed and input links (input angle) from the onset of the rake ( $t_0$ ) to the time of maximum neurocranial elevation and pectoral girdle retraction ( $t_{max}$ ) for (A) *Salvelinus* and (B) *Chitala*. Solid lines indicate link and angular positions at  $t_0$ , whereas stippled lines denote their positions at  $t_{max}$ . Input angles measured from data in previous kinematic studies (Sanford & Lauder, 1990; Sanford, 2001b; Konow et al. 2008). c, coupler link; f, fixed link; i, input link; o, output link.



an arc-shaped trajectory in *Salvelinus*, due to its partial insertion on the ventral surface of the third basibranchial before fully inserting on the first basibranchial (Fig. 3A). In *Chitala*, however, the short and stout CBL has a linear trajectory from its origin to a complete insertion on the medial side of the autogenous bony process of the second hypobranchial (Fig. 3F).

The pectoral girdle of *Salvelinus* can be compressed and extended in the dorsoventral plane due to the short cleithrum, which articulates dorsally with the supracleithrum (intrapectoral joint) at the level of the lateral line (Fig. 3). In contrast, the elongated cleithrum in *Chitala* results in an intrapectoral joint that is further dorsal, forming a more rigid dorsoventral bar on which the HP musculature inserts along the posterior face (Fig. 3D). Thus, pectoral girdle movement in *Chitala* is principally limited to an antero-posteriorly directed movement around the small, dorsally located supracleithrum. The post-temporal bone in *Salvelinus* has a single anterodorsal process that articulates with the occipital crest (Sanford, 2000), whereas in *Chitala* this bone has both anterodorsal and anteroventral processes (Taverne, 1978), possibly offering a more robust attachment of the pectoral girdle to the lateral pterotic region of the neurocranium.

An interesting suite of post-cranial specializations are present in *Chitala* (Fig. 3D–F; also in other notopterid knifefishes; see Taverne, 1978; Hilton, 2003), all of which are absent in *Salvelinus* (for post-cranial osteology in *Salvelinus*, see Lauder & Liem, 1980; Sanford, 2000). The pleural ribs in *Salvelinus* are dorsoventrally continuous and angled posteroventrally. In *Chitala*, they are dorsoventrally discontinuous (with the exception of the first two) and consist of true ribs and autogenous abdominal ribs (Hilton, 2003) that taper anteroventrally (Fig. 3F). The autogenous ribs in *Chitala* permit an independent anteroposterior movement of these ribs relative to the more dorsal true ribs and vertebral regions. A dense array of interlocking dermal scutes (Fig. 3D) limits anteroposterior compression of the ventral margin

of the body in this region (verified by manipulation of anaesthetized specimens). The first as well as the third to fifth anal pterygiophores are reduced and shortened, allowing the second, vastly hypertrophied, anal pterygiophore to move anteroposteriorly around its proximal articulation with the vertebral column (Fig. 3F). The anterior, pleural hypaxial musculature is sheet-like, whereas a belly-like ventral segment of this muscle connects the enlarged second anal pterygiophore with the coracoid. The caudal hypaxial musculature is more prominent and inserts primarily onto the hypertrophied second anal pterygiophore (Fig. 3F).

#### Sesamoid tendons in *Chitala*

Four distinct arrays of sesamoid tendons (the arête of Taverne, 1978) are found in the EP and HP musculature and along the vertebral column at the epaxial/hypaxial border: the epaxial array, dorsal vertebral array, ventral vertebral array and hypaxial array. Each array consists of two longitudinal series of bones, one on each side of the midline. The dorsal-most array, the epaxial sesamoid tendons, is distributed along the entire length of the body and arranged in a parasagittal plane. The dorsal vertebral sesamoid array is slightly ventral to the epaxial sesamoid tendons, extending posterolaterally at a 45° angle and partially overlapping the epaxial sesamoids. The ventral vertebral sesamoid array mirrors the dorsal vertebral array and the distribution of the ventral vertebral sesamoid array is restricted to the posterior region of the body, posterior to the second pterygiophore and extending posteriorly along the entire body. Lastly, the hypaxial sesamoid array is distributed midway between the vertebral column and the ventral margin of the body, extends posteriorly from the anterior margin of the dorsal fin to the caudal tip and is found directly superficial to the overlap between the true and abdominal ribs. These sesamoids have an almost horizontal orientation and are more densely packed than any of the other sesamoid arrays.

## Myology

In both species, the SH muscle originates from the anterior cleithrum and inserts onto the sesamoid urohyal and the dorso- and ventrohyal bones of the hyoid arch. The  $A_2A_3$  section of the AM originates on the posterolateral face of the suspensorium and inserts via a single stout tendon onto the coronoid process of the dentary (see also Lauder & Liem, 1980). In *Salvelinus*, the AM when viewed laterally has a smaller surface area compared with *Chitala* (not quantified but see Fig. 2A,C). The PIM in *Chitala* originates on the lateral face of the anterior ceratohyal with insertion onto the dentary at the mandibular symphysis and is elongate compared with its functional equivalent (Greenwood, 1971), the PH in *Salvelinus* (Fig. 2A,C). The EP muscles insert primarily onto the posterodorsal neurocranium in both species; however, some ventral EP fibres also insert onto the posterior edge of the supracleithrum. The ventral body musculature is composed of the HP muscles, which insert on the posterior cleithral and coracoid faces in both species and in *Salvelinus* also onto the supracleithrum, which is relatively larger in this species (Fig. 2A,C). In cross-section, the muscles of *Salvelinus* appear more spherical and robust compared with their homologues in *Chitala*, a pattern that is particularly pronounced in the EP musculature (Fig. 2B,D).

## Tongue-bite apparatus biomechanics

The MA of the third-order lever for neurocranial elevation was significantly lower in *Salvelinus* ( $t$ -test;  $P < 0.001$ ) than in *Chitala* (Table 3). By contrast, the mean DA was 4.8 in *Salvelinus*, significantly larger ( $t$ -test;  $P < 0.001$ ) than the mean DA of 3.2 in *Chitala*. The theoretical mean output force of the lever, being the product of EP ACSA ( $\text{mm}^2$ ) and MA of the lever, was 21 in *Salvelinus* compared with 23 in *Chitala* (Table 3) and did not differ significantly between

**Table 3** Species-means of mechanical coefficients of the third-order neurocranial lever and planar four-bar linkage in *Salvelinus* and *Chitala* based on osteological and myological measurements

	Mechanical coefficient	<i>Salvelinus</i>	<i>Chitala</i>
Neurocranial lever	Mechanical advantage	0.21	0.31
	Displacement advantage	4.76	3.23
	Theoretical output force	21.0	23.0
Planar four-bar linkage	Force transmission	0.44	0.51
	Kinematic transmission	2.26	1.95
	Output force factor	0.50	0.85

High values of mechanical advantage, force transmission and output force factor indicate an increase in output force or torque relative to the input force or torque. High values of displacement advantage and kinematic transmission indicate an increase in output velocity relative to the input velocity.

species ( $t$ -test;  $P = 0.37$ ). For the four-bar linkage model of hyoid retraction, *Salvelinus* had a FT of 0.44, a KT of 2.26 and an OFF of 0.50, whereas *Chitala* had an FT of 0.51, a KT of 1.95 and an OFF of 0.85 (Table 3).

## Statistical results

A PCA factoring 10 osteology and 10 myology variables returned a significant MANOVA (Wilks  $\lambda = 0.177$ ;  $f_{4,12} = 13.92$ ;  $P < 0.001$ ). Of the four PC axes with Eigenvectors  $> 1$  (Table 2), only PC1 demonstrated a significant species effect (ANOVA,  $P < 0.001$ ). This axis explained about 35% of the overall variance, and two-thirds of the 14 variables that loaded highly were osteological measurements. The TBA myology in *Salvelinus* was characterized by greater ACSA of the HP, EP and PH muscles (Table 2). Osteological measurements of inverse epaxial distance, TBA length, basihyal depth, cranial out-lever, and the coupler, output and fixed links were also all greater in *Salvelinus* (Table 2). In contrast, *Chitala* was found to have more massive AM and SH muscles as well as a longer cleithrum and input link than *Salvelinus*.

## Discussion

Both our qualitative and quantitative analyses established that all diagnostic TBA components, including basihyal dentition, opposing mouth-roof dentition and a CBL (Sanford, 2001b; Hilton, 2003), are present in *Salvelinus* and *Chitala*. We have also found that considerable interspecific differences exist in the mechanistic contribution from input motions of the neurocranium and pectoral girdle. Nevertheless, a convergent raking output motion results, involving inversely directed movement of the TBA jaws in order to immobilize and reduce captured prey (see Konow et al. 2008). Given this convergent raking kinematic output, the anatomical differences in the TBA are extraordinary; *Salvelinus* has an arc-shaped and elongate CBL and a priority on muscle strength and mechanical velocity amplification. Meanwhile, *Chitala* has a stout and straight CBL and a low priority on muscle force generation but increased mechanical force efficiency and velocity amplification, as well as additional post-cranial morphological specializations that may permit raking behavioural modulation. Below, we synthesize the available structural and functional data and discuss the structural and biomechanical basis for the evolution of interspecific differences in raking input movements, and how at the same time this has resulted in highly convergent raking output motions.

## Cleithrobranchial ligament morphology

The interesting relationships between TBA morphology and raking biomechanics are well reflected by the interspecific divergence in CBL morphology, which may be

integral to TBA function in raking, complementary prey-processing behaviours and alternative feeding behaviours such as suction feeding. The arc-shaped CBL in *Salvelinus* spans a longer origin/insertion trajectory between the pectoral girdle and hyoid bar than the comparatively straight ligament in *Chitala*, and its curvature in *Salvelinus* allows greater potential for changes in the distance between its origin and insertion during feeding (Fig. 3A–C). In the raking power-stroke, the CBL may transmit force and motion directly from the pectoral girdle to the basihyal. However, in *Salvelinus* this direct transfer of force will theoretically only be possible when the CBL is fully stretched (Fig. 3C). Although the CBL may be primarily straight in *Chitala*, CBL straightening in *Salvelinus* only occurs towards the end of the rake due to extensive neurocranium and pectoral girdle power-stroke excursion (Fig. 3C). This suggests that, in *Salvelinus*, a direct association exists between high-excursion kinematics (Sanford, 2001b) and the arc-shaped CBL morphology, although the relationship between these two remains unclear (see also Konow & Sanford, 2008b). Alternatively, *Salvelinus* may also rely on the SH to transmit strain from hypaxial-driven pectoral girdle retraction to retract the basihyal. However, previous evidence suggests that, during the power-stroke in *Salvelinus*, the SH muscle generates only low intensity activity (Konow et al. 2008). Future studies of a broader taxon sample from both raking lineages may clarify whether CBL morphology in general, and this ligament's capacity to structurally duplicate the SH in particular, directly influence the occurrence and extent of raking behavioural modulation and high-excursion kinematics.

### Tongue-bite apparatus myology

The robust TBA musculature in *Salvelinus* compared with *Chitala* suggests an emphasis on muscular power in the raking behaviour of *Salvelinus*. Given that ACSA and mass are directly proportional to the force production of a given muscle (Wainwright et al. 2004; Grubich, 2005), greater HP and EP ACSAs in *Salvelinus* (Table 2) indicate that forceful muscles are responsible for both the neurocranial elevation and pectoral girdle retraction driving the raking power-stroke in this and other morphologically similar salmonids (Sanford, 2001b; Konow & Sanford, 2008b). These power-stroke muscles provide *Salvelinus* with ample force to drive its high-excursion rakes with a neurocranial elevation of about 36°, one of the greatest observed in raking and in teleost feeding behaviours in general (Sanford, 2001b).

The PH also has a larger ACSA in *Salvelinus* (Table 2), thus corroborating the trend of more massive raking muscles in this taxon. When combined with a more robust TBA osteology (e.g. greater basihyal depth than in *Chitala*) (Table 2), this system in *Salvelinus* seems optimized for force production, causing substantial damage to the prey (Sanford, 2001b). Simultaneous priority on high force and

excursion is biologically rare (Anderson & Westneat, 2007) and this unusual strategy may be key for *Salvelinus* to successfully process a wide variety of prey despite its highly stereotyped raking behaviour (Sanford, 2001b; Grubich, 2003).

The more gracile muscles in *Chitala*, indicated by the smaller ACSA (Fig. 2C and Table 2), suggest a reduced force production potential, corresponding with comparatively more restricted kinematic excursions exemplified by a neurocranial elevation of only c. 11° in this taxon (Frost & Sanford, 1999; Sanford, 2001b; Konow et al. 2008). However, the SH and AM muscles in *Chitala* are exceptional (Table 2) in having a greater mass and thus force production potential (Wainwright et al. 2004; Grubich, 2005) than in *Salvelinus*. The SH is directly involved in basihyal retraction, with a modulated muscle activity pattern in response to prey-type differences, involving more intense recruitment during rakes on robust and elusive prey (Konow et al. 2008). Maintained oral jaw occlusion via prolonged AM contraction is a ubiquitous raking trait in osteoglossomorphs compared with salmonids (Sanford & Lauder, 1989; Konow & Sanford, 2008a; Konow et al. 2008).

### Post-cranial specializations in *Chitala*

Significant qualitative differences in TBA-related osteology are apparent in the post-cranial morphology of the study taxa. In *Chitala*, a range of anatomical specializations absent in *Salvelinus* may permit transmission of additional force for pectoral girdle retraction from the caudal HP. Increased cleithrum length (Table 2) and the resulting dorsal position of the intrapectoral joint (i.e. the cleithrum/supracleithrum junction) modify the pectoral girdle of *Chitala* into a dorsoventrally rigid bar (Fig. 3D). Conversely, flexion around the intrapectoral joint is more pronounced in *Salvelinus* (Fig. 3A–C), other salmonids and osteoglossid arowanas (Konow & Sanford, 2008b). The rigid pectoral girdle in *Chitala* [a structural synapomorphy of notopterid knifefishes (Hilton, 2003) and *Pantodon* (Taverne, 1974), their purported sister taxon (Lavoué & Sullivan, 2004)] is connected to the massive second anal pterygiophore via the sheet-like pleural HP. This muscle region is relatively anteroposteriorly incompressible, due to the presence of a dense row of ventral scutes, suggesting that isotonic contraction of the pleural HP is unlikely. However, the pleural region is capable of anteroposterior motion due to the presence of autogenous abdominal ribs that can move independently of the more dorsal ribs (Fig. 3D; see also Konow et al. 2008, online enhancement). Isotonic contraction of the caudal HP, most of which insert onto the hypertrophied second anal pterygiophore in notopterid knifefishes (Taverne, 1974), may facilitate strain transmission via the pleural HP and pectoral girdle to raking basihyal retraction. Although unquantified, this function of a highly derived and complex post-cranial morphological

character suite is supported by raking that relies primarily on pectoral girdle retraction in *Chitala* (Sanford & Lauder, 1990; Sanford, 2001a; Konow et al. 2008), despite the sheet-like pleural HP morphology in this species. The functional role of the extensive sesamoid tendon arrays in *Chitala* is unknown but interesting, as epaxial sesamoid tendons are found in other teleosts that also use neurocranial elevation during feeding despite a small EP muscle insertion area (viz. the Fistulariidae; S. Huskey, Western Kentucky University, Bowling Green KY pers. comm., 2008).

### Biomechanical models

The majority of the osteology variables responsible for interspecific differences (Table 2) were also integral components of the biomechanical models previously proposed to explain TBA function during raking (Konow & Sanford, 2008b). The neurocranial lever in *Salvelinus* involves a significantly greater DA, yielding almost a five-fold amplification of the input velocity (Grubich, 2005) compared with the corresponding system in *Chitala* where input velocity is only amplified three-fold (Table 3). The significantly greater MA of 0.3 in *Chitala* suggests a system with a greater priority on force production and more efficient force transmission than in *Salvelinus* with an MA of 0.2. Despite this, the theoretical output-force values for the neurocranial levers are similar between taxa (Table 3), suggesting that *Chitala* sacrifices velocity in favour of force amplification, whereas *Salvelinus* increases velocity without a significant decrease in force. The unusual mechanics that allow *Salvelinus* to amplify velocity without lowering force appear to result from the osteology of the neurocranial lever allowing a high DA and the large EP compensating for the inefficient force transmission resulting from the low MA of the lever. Therefore, when considering the osteology and myology of the neurocranial lever mechanism, the model suggests that neurocranial elevation in *Salvelinus* will be significantly faster, but no less forceful, than in *Chitala*. This notion is supported by kinematic data showing that the neurocranial elevation of *Salvelinus* during raking has a greater displacement and shorter duration to maximum excursion compared with *Chitala* (Sanford, 2001a).

Interestingly, in the hyoid four-bar linkage model of basihyal retraction, velocity transmission is approximately doubled for both taxa, with slightly greater amplification occurring in *Salvelinus* (Table 3). However, the output force of the system is much greater in *Chitala*, which has an OFF of 0.85 compared with 0.50 in *Salvelinus*. Given the similar FTs in both taxa, this difference appears to be driven by the significantly greater input link length in *Chitala* (Table 2). The emerging pattern is a mechanical emphasis on velocity in *Salvelinus*, coupled with a muscular emphasis on force. This contrasts with the mechanical system in *Chitala* where a greater priority is placed on force

transmission efficiency. Although muscular force is not transmitted as efficiently in *Salvelinus* as it is in *Chitala*, a considerable muscular potential for force production in *Salvelinus* results in rakes that are evidently both fast and powerful (Sanford, 2001a). These data support the hypothesis that modulation is not observed during raking in *Salvelinus* because the system is already optimized (Sanford, 2001a; Konow et al. 2008). Additionally, in *Salvelinus* the efficient transmission of velocity via the four-bar linkage (KT of 2.26 compared with 1.95 in *Chitala*) permits excursion along the coupler link (Suh & Radcliffe, 1978) and this may accomplish straightening of the CBL (Konow & Sanford, 2008a). As stated above, straightening of the CBL may allow a more direct transfer of strain from the pectoral girdle to the basihyal and ultimately increase the force of the raking power-stroke in *Salvelinus*.

Conversely, *Chitala* has a reduced capacity for muscular force, although this is amplified via the neurocranial lever, and the hyoid four-bar mechanics in this taxon favour velocity transmission. As velocity is considered crucial for efficient feeding on elusive prey (e.g. Westneat, 1994), it is reasonable to expect that *Chitala*, being a trophic specialist that feeds on elusive benthopelagic prey (Rahman, 1989; Lim et al. 1999), relies on velocity-amplifying raking mechanics. However, in both the neurocranial lever and the hyoid four-bar linkage, velocity amplification appears to be moderate and less than what is found in *Salvelinus*, a trophic generalist. This may be due to the low muscular force produced, which cannot withstand the sacrifice of force transmission efficiency that accompanies high velocity amplification.

Moreover, it is noteworthy that behavioural modulation of raking in *Chitala* involves an elastic recoil mechanism during processing of robust and elusive but not malleable and sedentary prey (Konow et al. 2008). In this way, *Chitala* may successfully process prey despite relatively modest mechanical force and velocity amplification by only applying maximum force and velocity to sufficiently challenging prey. In contrast, *Salvelinus* appears to optimize prey processing via a high-velocity mechanical system that is applied to all prey types.

Our analysis predicts that the TBA in *Salvelinus* allows high-velocity prey processing that is complemented by significant muscle force but in *Chitala* functions to mechanically conserve the force while maintaining the velocity amplification needed to process elusive prey. Although this corresponds well with the high-excursion and high-velocity kinematics of *Salvelinus* (Sanford, 2001a), it is interesting that these distinct mechanical systems between taxa appear to result in similar basihyal output kinematics (Konow et al. 2008). The divergent structural, mechanical and functional traits in *Salvelinus* and *Chitala* suggest that future analyses involving biomechanical quantification will be useful in explaining raking kinematic differences across a broader range of TBA-bearing taxa.

Although beyond the scope of this study, comparisons of predicted and realized motion patterns of the planar four-bar linkage for basihyal retraction will be necessary to identify and calibrate for deviations from the theoretical models such as link-length dynamics and discursion from two dimensions, which theoretically will significantly alter the transmission of force and motion in a four-bar linkage. Although neither is unprecedented in biological four-bars (Anker, 1974; Muller, 1987), it is unclear to what extent these discursions might impact the reliability of the model. Additionally, mechanical calculations, such as FT, KT and OFF, may change with four-bar orientation throughout the rake. However, calculations of the potential variation of mechanical properties of this system within a single rake were not possible with the data presented here but will be the subject of a forthcoming report.

### Summary

Morphology and biomechanics provide novel insights into the musculoskeletal basis for similarities and differences in raking behaviour of the study taxa (see Sanford & Lauder, 1989; Frost & Sanford, 1999; Sanford, 2001a,b; Konow et al. 2008). The TBA in *Salvelinus* is a robust musculoskeletal system with velocity-amplifying mechanics driven by larger muscles. This results in rakes that are unmodulated (a rare feature in trophic generalists) and are both forceful and fast. In contrast, the more gracile myology of the TBA in *Chitala* is restricted in its muscular force production. This restriction, however, is offset by mechanical force amplification in the neurocranial lever, whereas the hyoid four-bar linkage provides the velocity amplification necessary for processing elusive prey as well as efficient force transmission. *Chitala* also has several unique morphological features that enhance raking and allow modulation. It is clear that future studies of the biomechanical mechanisms and associated post-cranial morphology in a broader phylogenetic range of osteoglossomorphs and salmonids will clarify the functional and evolutionary diversification of this novel functional system.

### Acknowledgements

We thank Long Island Aquatics and Cold Spring Harbor Fish Hatchery for specimen sourcing and R. Petrizzo and V. Molina for help with dissections. This article was greatly improved by two anonymous reviewers and this work was supported by the National Science Foundation (IOS 0444891 and DBI 0420440 to C.P.J.S.).

### References

- Aerts P, Verraes W** (1984) Theoretical analysis of a planar four bar system in the teleostean skull: the use of mathematics in biomechanics. *Ann Soc R Belg* **114**, 273–290.
- Anderson PSL, Westneat MW** (2007) Feeding mechanics and bite force modelling of the skull of *Dunkleosteus terrelli*, an ancient apex predator. *Biol Lett* **3**, 76–79.
- Anker G** (1974) Morphology and kinetics of the head of the stickleback, *Gasterosteus aculeatus*. *Trans Zool Soc Lond* **32**, 311–416.
- Carroll AM** (2004) Muscle activation and strain during suction feeding in the largemouth bass *Micropterus salmoides*. *J Exp Biol* **207**, 983–991.
- Carroll AM, Wainwright PC, Huskey SH, Collar DC, Turingan RG** (2004) Morphology predicts suction feeding performance in centrarchid fishes. *J Exp Biol* **207**, 3873–3881.
- Frost BJ, Sanford CP** (1999) Kinematics of a novel feeding mechanism in the osteoglossomorph fish *Chitala chitala*: is there a prey-type effect? *Zoology* **102**, 18–30.
- Galis F** (2001) Key innovations and radiations. In *The Character Concept in Evolutionary Biology* (ed. Wagner GP), Ch. 25, pp. 581–605. San Diego: Academic Press.
- Greenwood PH** (1971) Hyoid and ventral gill arch musculature in osteoglossomorph fishes. *Bull Br Mus NatHist Zool* **19**, 257–285.
- Greenwood PH** (1973) Interrelationships of osteoglossomorphs. In *Interrelationships of Fishes* (eds Greenwood PH, Miles RS, Patterson C), pp. 307–332. London: Academic Press.
- Gregory WK** (1933) Fish skulls: a study of the evolution of natural mechanisms. *Trans Amer Philos Soc* **23**, 75–481.
- Grubich JR** (2003) Morphological convergence of pharyngeal jaw structure in durophagous perciform fish. *Biol J Linn Soc* **80**, 147–165.
- Grubich JR** (2005) Disparity between feeding performance and predicted muscle strength in pharyngeal musculature of black drum, *Pogonias cromis* (Sciaenidae). *Environ Biol Fish* **74**, 261–272.
- Hilton EJ** (2001) The tongue bite apparatus of osteoglossomorph fishes: variation of a character complex. *Copeia* **2001**, 372–382.
- Hilton EJ** (2003) Comparative osteology and phylogenetic systematics of fossil and living bony-tongue fishes (Actinopterygii, Teleostei, Osteoglossomorpha). *Zool J Linn Soc* **137**, 1–100.
- Konow N, Bellwood DR** (2005) Prey-capture in *Pomacanthus semicirculatus* (Teleostei, Pomacanthidae): functional implications of intramandibular joints in marine angelfishes. *J Exp Biol* **208**, 1421–1433.
- Konow N, Sanford CP** (2008a) Biomechanics of a convergently derived prey-processing mechanism in fishes: evidence from comparative tongue bite apparatus morphology and raking kinematics. *J Exp Biol* **211**, 3378–3391.
- Konow N, Sanford CP** (2008b) Is a convergently derived muscle-activity pattern driving novel raking behaviours in teleost fishes? *J Exp Biol* **211**, 989–999.
- Konow N, Camp AL, Sanford CP** (2008) Congruence between muscle activity and kinematics in a convergently derived prey-processing behaviour. *Integr Comp Biol* **48**, 246–260.
- Lauder GV** (1985) Aquatic feeding in lower vertebrates. In *Functional Vertebrate Morphology* (eds Hildebrand M, Bramble DM, Liem KF, Wake DB), pp. 210–229. Cambridge: Cambridge University Press.
- Lauder GV, Liem KF** (1980) The feeding mechanism and cephalic myology of *Salvelinus fontinalis*: form, function, and evolutionary significance. In *Charrs: Salmonid fishes of the genus Salvelinus* (ed. Balon EK), pp. 365–390. The Netherlands: Junk Publishers.
- Lauder GV, Liem KF** (1983) The evolution and interrelationships of the Actinopterygian fishes. *Bull Mus Comp Zool Harvard* **150**, 95–197.
- Lavoué S, Sullivan JP** (2004) Simultaneous analysis of five molecular markers provides a well-supported phylogenetic hypothesis for

- the living bony-tongue fishes (Osteoglossomorpha: Teleostei). *Mol Phylogen Evol* **33**, 171–185.
- Lim P, Lek S, Touch ST, Mao S-O, Chouk B** (1999) Diversity and spatial distribution of freshwater fish in Great Lake and Tonle Sap River (Cambodia, Southeast Asia). *Aquat Living Resour* **12**, 379–386.
- Muller M** (1987) Optimization principles applied to the mechanism of neurocranium levation and mouth bottom depression in bony fishes (Halecostomi). *J Theor Biol* **126**, 343–368.
- Rahman AKA** (1989) *Freshwater Fishes of Bangladesh Zoological Society of Bangladesh*. Dhaka: Department of Zoology, University of Dhaka.
- Ridewood WG** (1904) On the cranial osteology of the fishes of the families Mormyridae, Notopteridae, and Hyodontidae. *Zool J Linn Soc* **29**, 188–217.
- Rosen DE** (1974) Phylogeny and zoogeography of salmoniform fishes and relationships of *Lepidogalaxia salamandroides*. *B Am Mus Nat Hist* **153**, 265–326.
- Rosen DE** (1985) An essay on euteleostean classification. *Am Mus Novit* **2827**, 1–57.
- Sanford CP** (2000) *Salmonoid Fish Osteology and Phylogeny (Teleostei: Salmonoidei) Theses Zoologicae 33*. Liechtenstein: ARG Gantner Verlag KG.
- Sanford CP** (2001a) Kinematic analysis of a novel feeding mechanism in the brook trout *Salvelinus fontinalis* (Teleostei: Salmonidae): behavioral modulation of a functional novelty. *J Exp Biol* **204**, 3905–3916.
- Sanford CP** (2001b) The novel ‘tongue-bite apparatus’ in the knife-fish family Notopteridae (Teleostei: Osteoglossomorpha): are kinematic patterns conserved within a clade? *Zool J Linn Soc* **132**, 259–275.
- Sanford CP, Lauder GV** (1989) Functional morphology of the ‘tongue-bite’ in the Osteoglossomorph fish *Notopterus*. *J Morph* **203**, 379–408.
- Sanford CP, Lauder GV** (1990) Kinematics of the tongue-bite apparatus in osteoglossomorph fishes. *J Exp Biol* **154**, 137–162.
- Suh CH, Radcliffe CW** (1978) *Kinematics and Mechanisms Design*. New York: Wiley and Sons.
- Tao DC** (1967) *Fundamentals of Applied Kinematics*. Reading: Addison-Wesley.
- Taverne L** (1978) Ostéologie, phylogénèse et systématique des Téléostéens fossiles et actuels du super-ordre des Ostéoglossomorphs – Deuxième partie: Ostéologie des genres *Phareodues*, *Phareoides*, *Brychateus*, *Musperia*, *Pantodon*, *Singidia*, *Notopterus*, *Xenomystus* et *Papyrocranus*. *Académie Royal de Belgique, Mémoires de la Classe Des Sciences* **42**, 4–235.
- Thys T** (1997) Spatial variation in epaxial muscle activity during pry strike in largemouth bass (*Micropterus salmoides*). *J Exp Biol* **200**, 3021–3031.
- Wainwright PC** (1988) Morphology and ecology: functional basis of feeding constraints in caribbean labrid fishes. *Ecology* **69**, 635–645.
- Wainwright PC, Richard BA** (1995) Scaling the feeding mechanism of the largemouth bass (*Micropterus salmoides*): motor patterns. *J Exp Biol* **198**, 1161–1171.
- Wainwright PC, Bellwood DR, Westneat MW, Grubich JR, Hoey, AS** (2004) A functional morphospace for the skull of labrid fishes: patterns of diversity in a complex biomechanical system. *Biol J Linn Soc* **82**, 1–25.
- Westneat MW** (1994) Transmission of force and velocity in the feeding mechanisms of labrid fishes (Teleostei, Perciformes). *Zoomorphology* **114**, 103–118.
- Westneat MW** (2003) A biomechanical model for analysis of muscle force, power output and lower jaw motion in fishes. *J Theor Biol* **223**, 269–281.
- Westneat MW** (2004) Evolution of levers and linkages in the feeding mechanisms of fishes. *Integr Comp Biol* **44**, 378–389.